Tracer Kinetic Modeling: Basics and Concepts

20

Kjell Erlandsson

Contents

20.1 Introduction

In nuclear medicine, all studies are dynamic. Although most studies performed in nuclear medicine departments consist of a single static scan, the temporal dimension plays an important role in terms of the timing of the scan after administration of the tracer as well as its length.

In general, a radiotracer is administered by intravenous injection and clinical information is obtained from the uptake of the tracer in different organs and tissues. The uptake is determined by the delivery, retention and clearance of the tracer [1]. The delivery and clearance rates are dependent on the blood flow and the extraction of the tracer from blood to tissue while the retention is determined by metabolism of the tracer or binding of tracer molecules to specific or unspecific binding sites. All these processes are dynamic which, together with the physical decay of the radionuclide, leads to the tracer uptake chang-

K. Erlandsson (✉)
Institute of Nuclear Medicine, University College London, London, UK
e-mail: k.erlandsson@ucl.ac.uk

M. M. Khalil (ed.), *Basic Sciences of Nuclear Medicine*,
https://doi.org/10.1007/978-3-030-65245-6_20

ing over time in both concentration and spatial distribution. In order to determine quantitative parameters related to physiological or biochemical processes, it is necessary to determine the time-course of the tracer concentration in different organs and tissues. This can be done with a dynamic data acquisition protocol, consisting of a series of scans performed over a period of time from the administration of the radiotracer. Once sufficient knowledge has been accumulated regarding the kinetic behaviour of a certain tracer, it may be possible to develop simplified study protocols, which can provide relevant clinical information while being more patient friendly [2].

Having performed a dynamic acquisition, quantitative values for physiological or biochemical parameters can be determined by applying various mathematical tools to the data. This procedure is known as "kinetic analysis". Time–activity curves (TACs), representing the time-course of tracer concentration in the image, can be generated from dynamic PET or SPECT data. TACs can be obtained either for volumes of interest (VOIs) or for individual voxels, in the case parametric images are required. Absolute quantification of radioactivity is needed and therefore correction for physical effects such as attenuation, scatter, random coincidences (PET), and dead time are essential. Correction for partial volume effects (PVE) may also be needed. PVE correspond to contribution of information between adjacent image regions due to the limited spatial resolution in PET and SPECT [3]. Also, motion correction is obviously essential.

Kinetic analysis is done using a mathematical model of tracer behaviour [4], usually a compartmental model. In order to use such a model, it is necessary to have information about the tracer delivery in the form of an input function, ideally representing the time-course of tracer concentration in arterial plasma. This type of analysis can be useful within different clinical areas, such as cardiology, oncology and neurology, where tracers such as ^{15}O-H_2O, ^{18}F-FDG and ^{123}I-IBZM are used for quantification of blood flow, metabolic rate and neuroreceptor binding, respectively. In this chapter, we will describe the basic mathematical tools and concepts used in tracer kinetic modelling.

20.2 Compartmental Modelling

20.2.1 Definitions and Assumptions

In kinetic modelling theory, the term "steady state" is used for the situation when a certain parameter does not change with time. The term "equilibrium" is used for the situation when all compartments in a model are in steady state.

A series of assumptions are needed to proceed with tracer kinetic modelling. The most important of these are [5]:

1. The physiological processes that affect the measurements (e.g. blood flow) are in a steady state throughout the experiment.
2. The radio-ligands used are administered in tracer concentrations, and therefore do not affect the physiological or biochemical processes being studied.
3. The tracer concentration within a compartment is homogeneous—i.e. instantaneous mixing is assumed.

20.2.2 Compartmental Models

Physiological or biochemical systems are often described using compartmental models, in which a tracer is assumed to be transferred between a number of compartments, which can represent separate regions in space (e.g. vascular, interstitial or intracellular space), or alternatively different chemical states (e.g. parent compound, metabolic products or receptor bound tracer molecules). The rate of transfer from one compartment to another is proportional to the concentration in the compartment of origin and a first-order rate constant. In general, a compartmental model is described by a system of differential equations, where each equation corresponds to the sum of all transfer rates to and from a specific compartment:

$$\frac{\mathrm{d}}{\mathrm{d}t}C_i\left(t\right)=\sum_{\substack{j=1,..N\\ j\neq i}}\left(k_{ij}C_j\left(t\right)-k_{ji}C_i\left(t\right)\right);\quad i=1,\ldots N \tag{20.1}$$

where $C_i(\cdot)$ is the tracer concentration in compartment i, k_{ij} is the rate constant for transfer to

compartment i from compartment j, and N is the number of compartments in the model.

Compartmental models can be either reversible or irreversible. The irreversible models are those which contain at least one compartment that does not have an outflow.

In nuclear medicine, a single-index nomenclature is normally used to denote the rate constants. The rate constants for transfer from blood to tissue and from tissue to blood are called K_1 and k_2, respectively, and additional rate constants in the model are called k_3, k_4, etc. These symbols are sometimes qualified with asterisks or primes when necessary. Traditionally, a capital K is used in K_1, while lower case k:s are used for the other rate constants. This is to reflect a distinction in terms of units. While k_i, $i \geq 2$, are expressed in units of [min^{-1}], K_1 is expressed in same units as blood flow: [mL/min/mL] (mL of blood per minute per mL of tissue).

20.2.3 Solving Compartmental Models: The Laplace Transform

The Laplace transform is a useful tool when it comes to solving systems of linear first order differential equation, such as Eq. (20.1). The Laplace transform is defined as:

$$F(s) = \int_0^\infty e^{-st} f(t)\,dt \tag{20.2}$$

where s is a complex Laplace-space variable.

Using the properties listed in Table 20.1, it is possible to obtain solutions for complex compartmental systems. In particular, the property relating the transform of the derivative of a function to that of the original function is the key to the solution. After taking the Laplace transform of both sides in each equation, the terms are rearranged into the transform of a simple function, such as a sum of constants and exponential functions, and the inverse Laplace transform can then be found.

In the case of biological systems, the solution can often be expressed as:

Table 20.1 Laplace transform pairs

Time domain	Laplace domain
$f(t)$	$F(s)$
k	k/s
e^{kt}	1/(s-k)
$ag(t) + bh(t)$	$aG(s) + bH(s)$
$g'(t)$	$sG(s) - g(0)$
$g(t) \otimes h(t)$	$G(s)H(s)$

k, a and b are constants, t and s are variables, $g(\cdot)$, $G(\cdot)$, $h(\cdot)$ and $H(\cdot)$ are functions, $'$ represents derivative and $\otimes$ convolution

$$C_T(t) = H_N(t) \otimes C_a(t) \tag{20.3}$$

where $C_a(\cdot)$ and $C_T(\cdot)$ are the input and output functions, respectively, $\otimes$ represents the convolution operation and $H_N(\cdot)$ is the impulse response function (IRF) of the model, which has the following general form [6]:

$$H_N(t) = \sum_{i=1}^{N} \phi_i e^{-\theta_i t} \tag{20.4}$$

where ϕ_i and θ_i are functions of the individual rate constants of the model (K_1, k_2…), and N is the number of compartments. Irreversible compartments correspond to terms with $\theta_i = 0$, i.e. a constant. The number of terms in the impulse response function is equal to the number of compartments in the model.

Appendix 1 contains examples of Laplace transform derived solutions for different compartmental models. Sometimes it may be necessary to use the technique of partial fractions expansion [7] to find the individual terms of the impulse response function.

20.3 The 1-Tissue Compartment Model: Blood Flow

From a physiological point of view, the term "blood flow" refers to the volume of blood delivered to an organ per unit of time, often expressed in [mL/min], while "perfusion" refers to blood flow per unit of tissue-volume [mL/min/mL]. In the context of tracer kinetic modelling, the two terms are used interchangeably with the latter definition.

A model for quantifying blood flow was developed around the middle of the last century [8]. It was based on the Fick principle, which states that the rate of change of the tracer concentration in tissue is proportional to blood flow and to the difference in the arterial and venous concentrations:

$$\frac{\mathrm{d}}{\mathrm{d}t}C_{\mathrm{T}}(t) = F\left(C_{\mathrm{a}}(t) - C_{\mathrm{v}}(t)\right) \qquad (20.5)$$

where $C_{\mathrm{T}}(\cdot)$, $C_{\mathrm{a}}(\cdot)$ and $C_{\mathrm{v}}(\cdot)$ are the tissue, arterial and venous tracer concentrations, respectively, F is blood flow and t is time.

Assuming that the tracer concentration in tissue is at equilibrium with that in venous blood ($C_{\mathrm{T}}(t)/C_{\mathrm{v}}(t) = V_{\mathrm{D}}$), Eq. (20.5) can be rewritten as follows [9]:

$$\frac{\mathrm{d}}{\mathrm{d}t}C_{\mathrm{T}}(t) = FC_{\mathrm{a}}(t) - \frac{F}{V_{\mathrm{D}}}C_{\mathrm{T}}(t) \qquad (20.6)$$

The constant V_{D} is the "distribution volume" or "volume of distribution", representing the volume of tissue in which the tracer can move around freely. It is expressed in the units [mL/mL], i.e. mL per mL of tissue, and has a value in the range [0,1]. It is numerically equal to a quantity known as the partition coefficient.

The Kety–Schmidt model is only valid for tracers that are fully extracted from blood to tissue. This is true for many of the tracers used for measuring blood flow, such as ^{15}O-H_2O, ^{13}N-NH_4 and ^{133}Xe. On the other hand, if the tracer is not fully extracted (as in the case of e.g. ^{82}Rb), this may be taken into account using the extraction fraction, E, defined as the fraction of tracer extracted in a single pass through the capillary bed. The extraction fraction can be calculated using the Renkin–Crone formula [10, 11]:

$$E = 1 - \mathrm{e}^{-\mathrm{PS}/F} \qquad (20.7)$$

where PS is the permeability surface area product, expressed in the same unites as F [mL/min/mL]. (NB: E is dependent on F.)

Replacing F by FE in Eq. (20.6) and defining the constants $K_1 = FE$ and $k_2 = K_1/V_{\mathrm{D}}$ leads to:

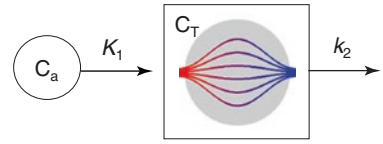

Fig. 20.1 The blood flow model (1-TC). C_{a} and C_{T} are the tracer concentrations in arterial blood and in tissue, respectively, and K_1 and k_2 are rate constants

$$\frac{\mathrm{d}}{\mathrm{d}t}C_{\mathrm{T}}(t) = K_1C_{\mathrm{a}}(t) - k_2C_{\mathrm{T}}(t) \qquad (20.8)$$

Equation (20.8) can be interpreted as the operational equation for a simple 1-compartment system (Fig. 20.1), and has the solution (see Appendix 1):

$$C_{\mathrm{T}}(t) = K_1\mathrm{e}^{-k_2t} \otimes C_{\mathrm{a}}(t) \qquad (20.9)$$

The model in Fig. 20.1 has in the past been referred to as a two-compartment model and represented with the arrow corresponding to k_2 directed from the tissue compartment back to blood. This may seem intuitively correct; however, it does not correspond to the actual mathematical relationship between the input and output functions. In practice, the input function is determined separately, and blood is not treated as a compartment in a mathematical sense. For clarity, it may therefore be appropriate to use a nomenclature, in which a model is named after the number of compartments used for describing the tracer distribution in tissue. Hereby, the model in Fig. 20.1 would be called a 1-tissue compartment (1-TC) model.

20.4 Multi-tissue Compartment Models: Neuroreceptor Mapping

Neuroreceptor mapping deals with studies of the systems that control the chemical transmission of neuronal signals across the synapse between two neurons. When an electrical impulse reaches the end of a presynaptic nerve cell, a series of events

are initiated: (1) Neurotransmitter substance is released from vesicles within the presynaptic cell into the synaptic cleft; (2) The neurotransmitter diffuses across to the postsynaptic cell where it binds to a specific type of receptors, triggering a new electrical impulse; (3) The neurotransmitter substance in the synapse is reabsorbed into the presynaptic cell via channels known as transporters, in order to prepare the synapse for the arrival of a new signal. In psychiatric studies, it is of interest to measure the concentration of different types of receptors or transporters in different brain regions. This can be achieved using radiotracers that bind selectively to the receptors or transporters of interest.

20.4.1 In Vitro Quantification

The theory for quantification of neuroreceptor binding in vivo is based on the theory for in vitro binding assays, which involves incubation of a receptor-enriched preparation with a radio-ligand. The basis for this theory is the law of mass action, which states that the ligand binds to receptors (association) at a rate proportional to the concentration of ligand and to the concentration of receptors, and that the resultant ligand-receptor complex breaks down (dissociation) at a rate proportional to the concentration of the complex [12]. This is described in the following equation:

$$\frac{\mathrm{d}}{\mathrm{d}t}[RL] = k_{\mathrm{on}}[R][L] - k_{\mathrm{off}}[RL] \quad (20.10)$$

where $[R]$, $[L]$ and $[RL]$ are the concentrations of receptors, ligand and receptor–ligand complex, respectively, and k_{on} and k_{off} are the rate constants for association and dissociation, respectively. Equation (20.10) can be represented as a simple two-compartment model with the rate constants $k_{\mathrm{on}}[R]$ and k_{off} (Fig. 20.2). In practice, $k_{\mathrm{on}}[R]$ can only be assumed to be constant if $[R] \gg [L]$ (tracer conditions).

During in vitro experiments, a state of equilibrium will be reached after a while, so that the rate of association is equal to the rate of dissociation, and the following relation is obtained:

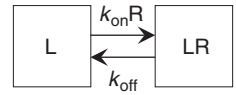

Fig. 20.2 The in vitro model. L, R and LR represent concentration of ligand, receptors, and ligand–receptor complex, respectively, and k_{on} and k_{off} are constants

$$k_{\mathrm{on}}[R][L] = k_{\mathrm{off}}[RL] \Leftrightarrow \frac{[R][L]}{[RL]} = \frac{k_{\mathrm{off}}}{k_{\mathrm{on}}} \equiv K_{\mathrm{D}} \quad (20.11)$$

The constant K_{D} is known as the equilibrium dissociation constant. Its reciprocal value is known as the affinity of the ligand for the receptor. Thus, a low K_{D} value corresponds to high affinity.

We now introduce a different set of symbols for free ligand, $F = [L]$, bound ligand, $B = [RL]$, and total receptor concentration, $B_{\max} = [R] + [RL]$. With these symbols we can rewrite Eq. (20.11) as follows:

$$B = \frac{B_{\max} F}{K_{\mathrm{D}} + F} \quad (20.12)$$

This is known as the Michaelis–Menten equation, and describes the relation between bound and free ligand equilibrium concentrations [13]. If B is plotted as a function of F, this equation corresponds to a saturation curve, which initially rises linearly ($B/F \approx B_{\max}/K_{\mathrm{D}}$, $F \ll K_{\mathrm{D}}$) and then gradually plateaus, asymptotically approaching a constant level ($B \approx B_{\max}$, $F \gg K_{\mathrm{D}}$). By measuring a series of corresponding B and F values, it is possible to estimate the parameters $B_{\max}$ and K_{D}. A simple solution is obtained using the Scatchard method [14], by plotting (B/F) versus B, which should give a straight line with a slope of $(-1/K_{\mathrm{D}})$ and an intercept of $(B_{\max}/K_{\mathrm{D}})$, as can be seen after rewriting Eq. (20.12) as follows:

$$\frac{B}{F} = \frac{B_{\max}}{K_{\mathrm{D}}} - \frac{1}{K_{\mathrm{D}}} B \approx \frac{B_{\max}}{K_{\mathrm{D}}} \equiv \mathrm{BP} \quad (20.13)$$

The first part of the above equation is valid for any values of B and F, while the second part is an approximation valid only under tracer conditions

($B \ll B_{max}$). The constant BP is the "binding potential" [15], which is an important parameter in in vivo neuroreceptor studies. As human in vivo studies are always performed under tracer conditions, in order to avoid pharmacological effects, it is not possible to estimate the values of B_{max} and K_D separately—only their ratio, BP, can be estimated.

20.4.2 In Vivo Quantification

The in vivo neuroreceptor model is a combination of the two models discussed above; the blood flow model and the in vitro binding assay model. Apart from specific binding to receptors, most tracers will also exhibit so-called nonspecific binding, involving macromolecules such as proteins. Nonspecific binding is not saturable and not displaceable. A general neuroreceptor model therefore requires three tissue compartments (see Fig. 20.3), and can be described as follows:

$$\begin{cases} \frac{\mathrm{d}}{\mathrm{d}t}C_F(t) = K_1 C_p(t) + k_4 C_S(t) + k_6 C_{NS}(t) - \\ \qquad\qquad (k_2 + k_3 + k_5) C_F(t) \\ \frac{\mathrm{d}}{\mathrm{d}t}C_S(t) = k_3 C_F(t) - k_4 C_S(t) \\ \frac{\mathrm{d}}{\mathrm{d}t}C_{NS}(t) = k_5 C_F(t) - k_6 C_{NS}(t) \end{cases} \tag{20.14}$$

where $C_p(\cdot)$, $C_F(\cdot)$, $C_S(\cdot)$ and $C_{NS}(\cdot)$ are the tracer concentrations in plasma and in the compartments for free, specifically bound and nonspecifically bound tracer, respectively, and K_1, k_2–k_6 are rate constants.

With six free parameters (K_1, k_2–k_6) the 3-TC model is normally too complex to be useful in practical situations. All the parameters may not be identifiable,[1] given the limited amount of information available (one single TAC represents the sum of all tissue compartments) and the presence of noise in the measured data. Therefore, it is often necessary to reduce the complexity of the model by reducing the number of compartments. The 3-TC model would thereby be converted to a 2-TC or even a 1-TC model. At this point, it is important to note that when the compartmental structure of a model changes, so does the meaning of the rate constants. It may therefore be appropriate to use different symbols in different models. Hence, in the 2-TC model, k_2 and k_3 become k_2' and k_3', and in the 1-TC model, k_2 becomes k_2'' [17]. When dealing with a single model, such distinction may not be necessary, however.

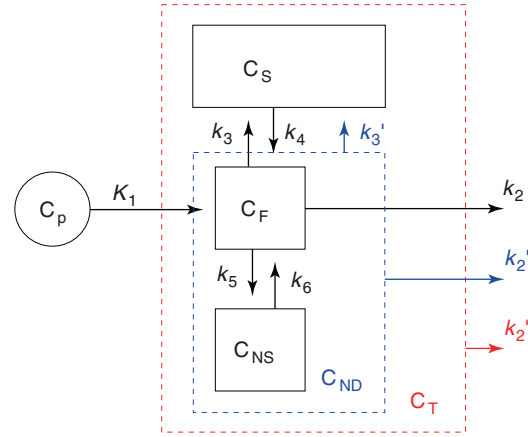

Fig. 20.3 Combined illustration of the 3-TC, 2-TC and 1-TC models for neuroreceptor quantification. C_p is the concentrations of unmetabolised tracer in plasma, C_F, C_{NS} and C_S are the concentrations of free, nonspecifically bound and specifically bound tracer in tissue, respectively, C_{ND} is the concentration of non-displaceable tracer in tissue ($C_{ND} = C_F + C_{NS}$), and C_T is the total concentration of tracer in tissue. The sets of rate constants used in the different models are: $\{K_1, k_2–k_6\}$ (3-TC), $\{K_1, k_2', k_3', k_4\}$ (2-TC) and $\{K_1, k_2''\}$ (1-TC model)

In the 2-TC model (Fig. 20.3, blue components) the free and nonspecific binding compartments are merged into the so-called "non-displaceable" (ND) compartment. The 2-TC model can be described as follows:

$$\begin{cases} \frac{\mathrm{d}}{\mathrm{d}t}C_{ND}(t) = K_1 C_p(t) + k_4 C_S(t) \\ \qquad\qquad -(k_2' + k_3') C_{ND}(t) \\ \frac{\mathrm{d}}{\mathrm{d}t}C_S(t) = k_3' C_{ND}(t) - k_4 C_S(t) \end{cases} \tag{20.15}$$

[1] Parameter identifiability means that a change in the parameter values should always lead to a change in the output function [16].

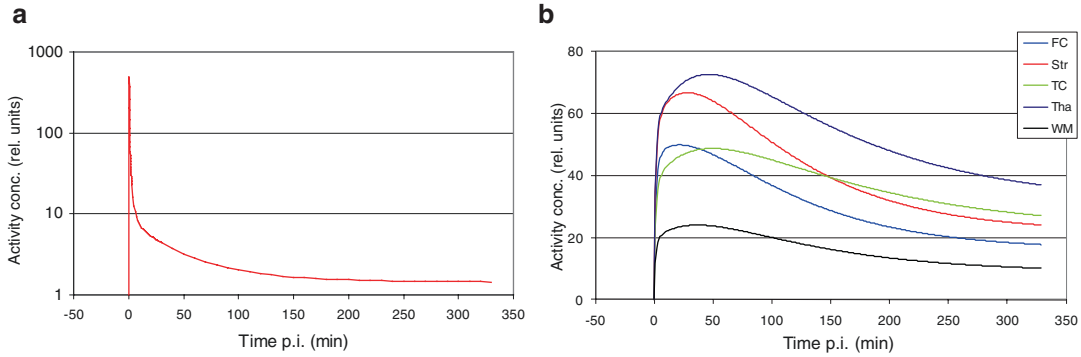

Fig. 20.4 Time–activity curves corresponding to the NMDA receptor SPECT tracer ^{123}I-CNS 1261 with bolus injection; (**a**) arterial plasma input function, (**b**) tissue curves for various brain regions: Frontal cortex (FC), striatum (Str), temporal cortex (TC), thalamus (Tha) and white matter (WM)

where $C_{ND}(\cdot)$ is the total tracer concentration in the nondisplaceable compartment, and k_2' and k_3' are rate constants specific to this model.

This simplification implicitly involves the assumption that equilibrium is rapidly established between the F- and NS-compartments, and that the free fraction in tissue, f_{ND}, is constant during the experiment. f_{ND} is defined as:

$$f_{ND} = \left[\frac{C_F}{C_F + C_{NS}}\right]_{eq} = \frac{k_6}{k_5 + k_6} \quad (20.16)$$

The last equality is obtained by setting $dC_{NS}(t)/dt$ in Eq. (20.14) to 0 (equilibrium). The tissue free fraction, f_{ND}, cannot be measured directly. The relationships between the rate constants in the 2-TC and 3-TC models can be derived by equating the transport rates between compartments in the two models, resulting in:

$$k_2' = f_{ND} k_2; \quad k_3' = f_{ND} k_3 \quad (20.17)$$

In the 1-TC model (Fig. 20.3, red components), one single compartment represents non-displaceable and specifically bound tracer in tissue. It can be described by a single differential equation:

$$\frac{d}{dt} C_T(t) = K_1 C_p(t) - k_2'' C_T(t) \quad (20.18)$$

where $C_T(\cdot)$ is the total concentration of non-displaceable and specifically bound tracer in tissue, and k_2'' is a rate constants specific to this model. As above we obtain:

$$k_2'' = k_2' \left(\frac{k_4}{k_3' + k_4}\right) = k_2' \left(1 + \frac{k_3'}{k_4}\right)^{-1} \quad (20.19)$$

The 1-TC model for neuroreceptor quantification is mathematically equivalent to the one used for blood flow above (Fig. 20.1). The difference is that, while the main parameter of interest in the case of blood flow measurements is the uptake rate constant, $K_1 = FE$, in the case of neuroreceptor studies, the main parameter of interest is the washout rate constant, k_2'', which reflects the amount of tracer retention in tissue due to receptor binding (sometimes quantified by the parameter $BP_{ND} = k_3'/k_4$ (see below)).

Figure 20.4 shows an example of TACs corresponding to a SPECT study using the NMDA receptor tracer [^{123}I]CNS-1261 [18]. The tissue curves were generated with the 2-TC model using averaged rate constants (Table 20.2).

20.5 Input Function

In vivo quantification requires knowledge of the time-course of tracer concentration in arterial plasma, $C_p(t)$, referred to as the arterial input function (AIF). Traditionally, the AIF is obtained by repeated arterial sampling throughout the experiment. The samples first need to be centrifuged, in order to separate plasma and blood cells, and estimate the plasma-to-whole blood concentration ratio (f_{pob}).

Table 20.2 Averaged rate constants for the 2-TC model for the SPECT tracer [^{123}I]CNS-1261

	K_1 (mL/min/mL)	k_2' (min^{-1})	k_3' (min^{-1})	k_4 (min^{-1})
FC	0.172	0.023	0.018	0.036
Str	0.215	0.018	0.016	0.058
TC	0.145	0.019	0.039	0.037
Tha	0.227	0.033	0.106	0.049
WM	0.076	0.025	0.078	0.075

FC frontal cortex, *Str* striatum, *TC* temporal cortex, *Tha* thalamus, *WM* white matter

A factor that complicates the quantification procedure is the presence of radioactive metabolites, produced in peripheral organs (liver, kidneys, lungs, etc.), and released back into the blood stream. If the metabolites can cross the blood–brain barrier (BBB), it would be necessary to use a more complex model with more parameters, resulting in increased variability. This problem can be avoided by appropriate tracer selection. However, radioactive metabolites in the blood stream can in general not be avoided, and metabolite correction of the AIF is therefore needed. For this purpose, high-pressure liquid chromatography (HLPC) can be used to determine the fraction of radioactivity in arterial plasma corresponding to un-metabolised tracer. This "plasma parent fraction" (f_{pp}) starts at 1 for $t = 0$ and decreases with increasing time at a rate that depends on the tracer and on the individual subject. In order to apply a correction, measured data points are fitted with an analytical function, such as e.g. a bi-exponential or the Hill function: $f_{pp}(t) = 1 + (a - 1) \bullet t^b/(c + t^b)$, where a, b and c are parameters to be optimised. For a comprehensive list of functions used for different tracers, see [19].

The measured input function is also affected by nonspecific binding in plasma. Tracer bound to protein molecules is not available for transportation across the BBB. Usually it is assumed that equilibrium is reached quickly between free and protein-bound tracer in plasma, and the free fraction in plasma, f_p, is thereby assumed to be constant during the experiment. It is possible to measure f_p (e.g. by ultrafiltration), but these measurements can have high variability, and this factor is often ignored. The concentration of free parent compound in arterial plasma can thus be obtained as follows:

$$C_{p,F}(t) = f_p C_p(t) = f_p \cdot f_{pp}(t) \cdot f_{pob}(t) \cdot C_a(t) \tag{20.20}$$

where f_p is the plasma free fraction (assumed constant), $f_{pp}(\cdot)$ the plasma parent fraction, $f_{pob}(\cdot)$ the plasma over whole blood ratio, $C_p(\cdot)$ the total concentration of parent compound in plasma, and $C_a(\cdot)$ the total arterial activity concentration.

Arterial sampling is an invasive and labour-intensive procedure, and it would be a clear advantage if it could be avoided. In some cases, the input function can be obtained directly from the images, if an appropriate blood pool can be identified. This is known as an image derived input function (IDIF) [20]. In thoracic studies, the heart ventricles or the aorta can be used to obtain an IDIF. In brain studies, the carotid arteries can be used but, as they are relatively small, accurate partial volume correction is needed [21]. Also, when using an IDIF, it may be necessary to take a few blood samples for metabolite and plasma-to-whole blood correction, but these samples could be venous samples rather than arterial.

20.6 Outcome Measures

The most fundamental parameters in compartmental modelling are the rate constants (K_1, k_2…). These so-called micro-parameters can usually not be determined with a high degree of precision (apart from K_1), due to noise present in the data (mainly related to limited counting-statistics in the photon detection process). Therefore various so-called macro-parameters are usually determined, by combining two or more micro-parameters, in order to obtain more robust outcome measures. For reversible tracers, the macro-parameters of interest are the total volume of distribution (V_T) and the binding potential (BP), and for irreversible tracers it is the influx rate (K_i).

20.6.1 Total Volume of Distribution

One of the most robust outcome measure is the "total volume of distribution", V_T, defined as the ratio between tracer concentration in tissue and

in plasma at equilibrium. V_T is expressed in units of [mL/mL]. V_T is useful in neuroreceptor studies since it is dependent on the receptor concentration in the target tissue but independent of blood flow (see below). In theory, it corresponds to the integral of the impulse response function of the model [6].

When using compartmental modelling, V_T can be calculated from the rate constants with expressions derived by equilibrium-analysis of the differential equations that describe each model. Thus we obtain the following expressions for the 3-TC, 2-TC and 1-TC models:

$$V_T = \left[\frac{C_T(t)}{C_p(t)}\right]_{eq} = \frac{K_1}{k_2}\left(1+\frac{k_3}{k_4}+\frac{k_5}{k_6}\right) = \frac{K_1}{k_2'}\left(1+\frac{k_3'}{k_4}\right) = \frac{K_1}{k_2''} \tag{20.21}$$

This equation shows that V_T is independent of blood flow: Both K_1 and k_2 depend on blood flow, but their ratio does not, and neither do the rate constants k_3–k_6.

The use of the term "volume of distribution" for quantification of tracer binding may seem a bit confusing. It is used for historical reasons as its calculation is similar to that of the actual distribution volume of a tracer that exhibits neither specific nor nonspecific binding (see blood flow section above). As an afterthought, it may be interpreted as the volume of plasma containing the same total activity as 1 mL of tissue.

20.6.2 Binding Potential

The principal outcome measure in neuroreceptor studies is the binding potential, BP, but in practice it can be difficult to estimate BP according to the definition in Eq. (20.13). In the past several alternative definitions were used, which would sometimes lead to confusion. Therefore, a consensus was reached among researches in the field, and three different types of in vivo binding potentials definitions were proposed: BP_F, BP_p and BP_{ND} [22]. All three are defined in terms of the ratio at equilibrium of the concentration of specifically bound tracer (C_S) vs. a reference concentration. The difference between the three lies in the reference used. For BP_F, it is the free tracer concentration in plasma ($C_{p,F} = f_p C_p$), which at equilibrium is equal to the free concentration in tissue ($C_F = f_{ND} C_{ND}$); for BP_p, it is the total concentration of parent compound in plasma (C_p); and for BP_{ND}, the concentration of non-displaceable tracer in tissue (C_{ND}).

Another difference with in vitro studies is that in vivo measurements do not reflect the total receptor concentration, B_{max}. Some fraction of the receptors may be occupied by the endogenous transmitter substance (dopamine, serotonin…), by some drug administered to the patient, or by the tracer itself. In vivo studies reflect the concentration of available receptors, B_{avail}.

As in the case of V_T, the various BP-values can be derived from the model parameters. Also, if a brain region exists that is known not to have any specific binding, this can be used as a reference region with the volume of distribution V_{ND}. BP-values can then be derived from V_T and V_{ND} values. This approach usually yields more robust results as compared to estimating the BP-values directly from the rate constants. The relationships between BP, V_T and model parameters is summarised below and illustrated in Fig. 20.5.

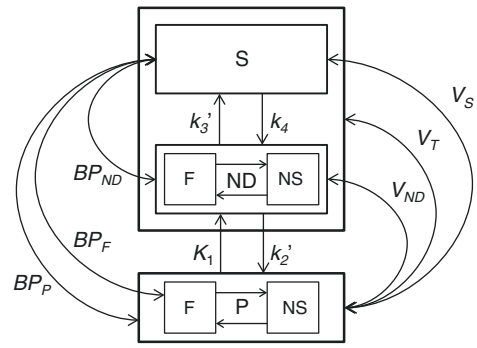

Fig. 20.5 Illustration of the relationships between various binding potentials (BP_X) and volumes of distribution (V_X). (NB: $BP_p = V_S = V_T - V_{ND}$)

$$\mathrm{BP_F} \equiv \frac{B_{\mathrm{avail}}}{K_\mathrm{D}} = \left[\frac{C_\mathrm{S}}{C_{\mathrm{p,F}}}\right]_{\mathrm{eq}} = \left[\frac{C_\mathrm{S}}{C_\mathrm{F}}\right]_{\mathrm{eq}} = \frac{k_3}{k_4}$$

$$\mathrm{BP_p} \equiv \left[\frac{C_\mathrm{S}}{C_\mathrm{p}}\right]_{\mathrm{eq}} = f_\mathrm{p} \cdot \mathrm{BP_F} = \frac{K_1}{k_2'}\frac{k_3'}{k_4} = V_\mathrm{T} - V_\mathrm{ND}$$

$$\mathrm{BP_{ND}} \equiv \left[\frac{C_\mathrm{S}}{C_\mathrm{ND}}\right]_{\mathrm{eq}} = f_\mathrm{ND} \cdot \mathrm{BP_F} = \frac{k_3'}{k_4} = \frac{V_\mathrm{T} - V_\mathrm{ND}}{V_\mathrm{ND}} \tag{20.22}$$

Of the three in vivo BP-measures, $\mathrm{BP_F}$ is the one that comes closest to the in vitro definition in Eq. (20.13), but it can be difficult to determine in practice. The use of $\mathrm{BP_p}$ requires the assumption that f_p is constant between scans or across groups of subjects. $\mathrm{BP_{ND}}$ requires the same assumption regarding f_ND, but has the advantage that it can be estimated using the reference tissue model, which does not require arterial sampling (see below).

It is generally assumed that a change in BP reflects a change in B_{avail}. Thereby, the fraction of receptors occupied by a drug (occupancy, O) can be estimated by measuring BP before ($\mathrm{BP_{base}}$) and after giving the drug ($\mathrm{BP_{drug}}$) [22]:

$$O \equiv 1 - \frac{B_{\mathrm{avail,drug}}}{B_{\mathrm{avail,base}}} = 1 - \frac{\mathrm{BP_{drug}}}{\mathrm{BP_{base}}} \tag{20.23}$$

where BP in $\mathrm{BP_{base}}$ and $\mathrm{BP_{drug}}$ can be either $\mathrm{BP_F}$, $\mathrm{BP_p}$ or $\mathrm{BP_{ND}}$.

20.7 Parameter Estimation

20.7.1 AIF Models

Once the AIF has been determined and the IRF of the model has been defined, the individual parameters (K_1, k_2...) can be estimated. This is an inverse problem, where an equation of type (Eq. 20.3) represents the forward model, and which can be solved using an iterative procedure, such as the Levenberg–Marquardt algorithm [23]. The goal is to minimise the difference between the measured data (TAC) and the model output function in a least-squares sense. Usually, some kind of weighting scheme is used before combining the data from different time points, to take into account differences in variability due to the changing activity concentration and difference in the length of each timeframe. It is necessary to take into account the fact that a measured tissue TAC will always contain a contribution from blood. This can be done by estimating an extra parameter, representing the blood volume (V_b), or by assuming it is constant (e.g. $V_\mathrm{b} = 5\%$). It is important to remember that the total arterial concentration should be used in this term.

The forward model can be implemented using either an analytic solution for the IRF or a numerical calculation based on the differential equations, with e.g. the Runge–Kutta method [24].

20.7.2 Simultaneous Estimation

As an alternative, the input function can be built into the model itself, utilising the fact that different tissue regions have the same AIF. In this case, the AIF is described by an analytical function with a number of parameters, which are estimated simultaneously with those of several tissue TACs [25]. These TACs should be as different from each other as possible. A bonus with this method is that no metabolite correction is needed.

20.7.3 Reference Tissue Models

Another approach, which is often used in brain studies, is the reference tissue model. Here the TAC for a brain region, devoid of specific binding (reference region), is used as an indirect input function. Two alternative models that have been proposed are: The full reference tissue model (FRTM) [26, 27], based on the 2TC-model, and the simplified reference tissue model (SRTM) [28], based on the 1-TC model (see Fig. 20.6). The IRFs for these models are derived in Appendix 2.

In principle FRTM is dependent on the six rate constants: K_1, k_2', k_3', k_4, ${}^R K_1$ and ${}^R k_2'$, where the first four belong to the target region and the latter two to the reference region. However, K_1 and ${}^R K_1$ only appear in the model equation as a ratio: $R_1 = K_1/{}^R K_1$. Furthermore, it can be assumed that

the volume of distribution of the non-displaceable compartment (V_{ND}) is the same for both regions: $K_1 / k_2' = {}^R K_1 / {}^R k_2' \Leftrightarrow k_2' = R_1 {}^R k_2'$, and thereby the number of model parameters can be reduced to four. SRTM has the following three parameters: R_1, k_2'' and ${}^R k_2'$. A method for noise-reduction in SRTM has been proposed, taking into account the fact that ${}^R k_2'$ should be independent of the target region analysed [29].

As an illustration, Fig. 20.7 shows simulated data corresponding to the SPECT tracer ^{123}I-ADAM, which binds to serotonin transporters (presynaptic reuptake channels; 5-HTT), and can be used for measuring occupancy of antidepressant drugs. The data were generated based on averaged parameters obtained with SRTM [30]. Time–activity curves are shown for the midbrain, which is the region with highest 5-HTT concentration, and for cerebellum, which was the reference region. The parameters used were: $R_1 = 0.85$, ${}^R k_2' = 0.030\,\text{min}^{-1}$ and $BP_{ND} = 1.14$.

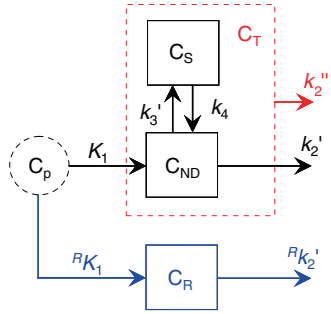

Fig. 20.6 Combined illustration of the full and the simplified reference region models. C_p is the (unknown) concentrations of non-metabolised tracer in plasma, C_{ND} and C_S are the concentrations of non-displaceable and specifically bound tracer in the target tissue, respectively, C_T is the total concentration of tracer in tissue, and C_R is the tracer concentration in the reference region. The sets of rate constants corresponding to the full and simplified models are: $\left\{K_1, k_2', k_3', k_4, {}^R K_1, {}^R k_2'\right\}$ and $\left\{K_1, k_2'', {}^R K_1, {}^R k_2'\right\}$, respectively

20.7.4 Spectral Analysis

From Eqs. (20.3) and (20.4) we obtain:

$$C_T(t) = C_p(t) \otimes \sum_{i=1}^{N} \phi_i e^{-\theta_i t} = \sum_{i=1}^{N} \phi_i \left(C_p(t) \otimes e^{-\theta_i t} \right) = \sum_{i=1}^{N} \phi_i \psi_i(t)$$

In the method of spectral analysis [31], a library of basis-functions, $\psi_i(t)$, is first generated for a suitable range of θ_i values. The problem is then solved using a non-negative least-squares fitting algorithm, resulting in a limited number of components, with non-zero coefficients, ϕ_i. The number of non-zero components corresponds to the number of model compartments, which therefore does not need to be fixed beforehand. (Two adjacent non-zero coefficients, ϕ_i and ϕ_{i+1} should in this context be regarded as

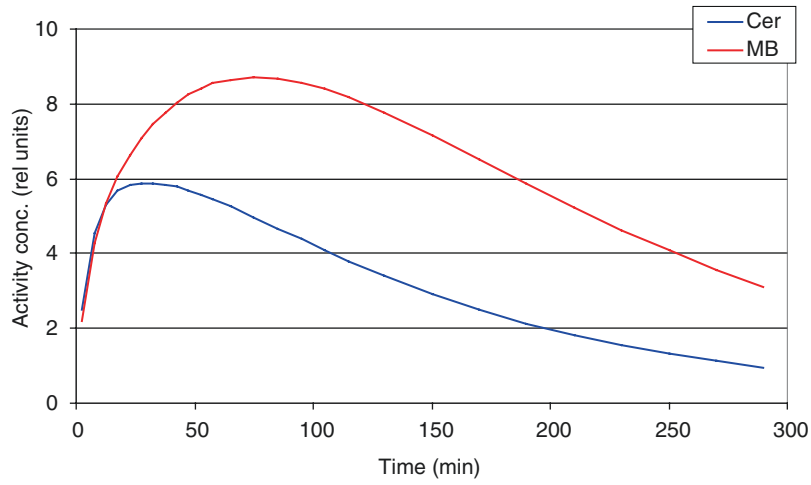

Fig. 20.7 Time–activity curves for the 5-HTT SPECT tracer ^{123}I-ADAM. The two curves represent midbrain (MB) and cerebellum (Cer), which was used as a reference region

one single component, with a θ value somewhere between θ_i and θ_{i+1}.)

The spectral analysis method is not strictly valid for reference tissue models, where negative components in theory can occur. Therefore a more general method was developed using the basis pursuit technique [32].

20.7.5 Graphical Analysis

An alternative approach to compartmental modelling can be found after integrating the differential equations describing the kinetic models. This yields equations which lend themselves to graphical analysis. The basic idea is that, after an appropriate transformation, the data can be plotted as a graph and a straight line fitted to the points. The slope and intercept of the fitted line will reflect certain characteristics of the tracer uptake or binding. The Logan method [33] was developed specifically for reversible tracers, and is obtained by plotting $y(t) = \int_0^t C_T(\tau)\,d\tau / C_T(t)$ vs. $x(t) = \int_0^t C_p(\tau)\,d\tau / C_T(t)$. After some time ($t^*$), a straight line is obtained with a slope equal to V_T. This result is independent of the assumed compartmental structure of the model, as shown in Appendix 3.

This approach is also known as linearisation, since it converts a nonlinear parameter estimation problem into a linear one. For this reason, it is also quite fast, and thereby useful in voxel-based analysis. A limitation of the approach is that it may result in bias with noisy data due to correlation in the noise structure between the dependent and independent variables [34]. A more robust approach has been proposed [35]. A reference region version of the Logan method has also been developed [36].

There is a corresponding method for irreversible tracers, known as the Patlak plot [37]. Here $y(t) = C_T(t)/C_p(t)$ is plotted vs. $x(t) = \int_0^t C_p(\tau)\,d\tau / C_p(t)$, and the slope of the linear part of the curve (after equilibrium has been reached) is the influx rate, $K_i = K_1 \cdot k_3/(k_2 + k_3)$. The intercept is the sum of the blood volume, V_b, and the reversible volume of distribution, $V_D = K_1 \cdot k_2/(k_2 + k_3)^2$. The method can be described by an uncoupled 2-TC model with one reversible and one irreversible compartment (Fig. 20.8). This approach is often used for analysis of ^{18}F-FDG data, including the dynamic whole-body imaging technique, based on a multi-pass, multi-bed acquisition protocol [38].

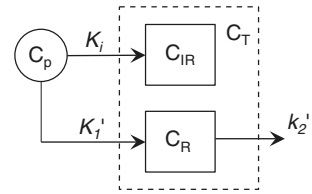

Fig. 20.8 Illustration of the Patlak model. C_p is the concentration of tracer in plasma, C_R and C_{IR} the concentrations of reversible and irreversible tracer uptake, respectively, and C_T is the total concentration of tracer in tissue. The rate constants are: $K_i = K_1 \cdot k_3/(k_2 + k_3)$, $K_1' = K_1 \cdot k_2/(k_2 + k_3)$ and $k_2' = k_2 + k_3$. The outcome parameters are the irreversible uptake rate, K_i, and the reversible volume of distribution, $V_D = K_1'/k_2'$

20.7.6 The Bolus/Infusion Approach

In conventional studies, the tracer is administered with a single injection over a short time period—a so-called "bolus injection". An alternative approach is to use a constant infusion protocol, where tracer is being continuously administered slowly throughout the experiment. The aim is to establish a true equilibrium situation, which allows for direct estimation of V_T as the ratio of tissue and plasma activity concentration, in accordance with the definition (Eq. 20.21) [39]. Equilibrium can be reached more rapidly by using a combination of constant infusion and an initial bolus injection (a "bolus/infusion", B/I, protocol) [40]. This approach is particularly useful in "challenge studies", in which the radiotracer is displaced by a cold competitor. It is also useful in situations when a linear model is not applicable, such as in the case of "multiple ligand concentration receptor assays" [41, 42]. In these

studies, low concentration of the radio-ligand is used in order to estimate B_{max} and K_D separately. A B/I paradigms was also used in order to avoid arterial sampling by replacing it with venous sampling at equilibrium with the SPECT tracer [^{123}I]CNS-1261 [43].

20.7.7 Model Comparison

Choosing a quantification method involves a trade-off between bias, variance and practicality. A model with more parameters will always give a better fit to the data (as judged by the residual sum of squares), but this may be because it is fitting the noise in the data rather than the actual signal. A model with less parameters will lead to less variability in the results, but can also lead to bias, if the model does not properly describe the underlying physiological or biochemical processes. There are various statistical methods for determining the best model, based on the residuals of the fit and on the number of parameters [44–46]. In principle, these methods correspond to application of the old philosophical principle known as "Occam's razor". If two models can describe the data equally well,[2] the best model is the simplest one.

The use of various different models and comparison of the estimated outcome measures is an approach that has been recommended in order to avoid systematic errors related to one particular model. In terms of practicality, it may be appropriate to also consider methods based on simplified data acquisition protocols, such as reference tissue methods, bolus/infusion methods or even single scan protocols. However, these methods should always first be validated versus more complex and accurate ones (see e.g. [47]).

20.8 Applications: Schizophrenia

PET and SPECT studies have been used for many years in psychiatric research. A wide range of tracers have been developed for imaging different neurotransmitter (especially dopamine and serotonin) systems. These tracers have allowed for studies which aid in the drug development process by providing information on drug delivery, mechanism of action and occupancy levels at targets of interest. Below we present some illustrative examples, based on work from the research career of the late Prof. Lyn S Pilowsky.

Antipsychotic drugs are used for treatment of schizophrenic patients, and their therapeutic effect is believed to be related to blockade of postsynaptic dopamine D_2-receptors. They can be classified into two groups: Typical and atypical (or first and second generation) drugs. The atypical antipsychotics are advantageous in that they produce less Parkinsonian side effects than the typical ones, while preserving high clinical efficacy. Pilowsky et al. [48] used the SPECT tracer ^{123}I-IBZM to compare the atypical drug Clozapine with the typical drug Haloperidol. They showed that Clozapine produced a lower level of D_2/D_3 receptor blockade in the striatum (a central brain structure), which would explain the lower level of Parkinsonian side effects.

Different theories emerged regarding the mechanism of action of atypical drugs, involving either different receptor types or different brain regions. To investigate the importance of blocking serotonin-(5-HT) 2A receptors, Travis et al. [49] used the SPECT tracer ^{123}I-R91150, and found no correlation between clinical efficacy of atypical antipsychotics and 5-HT_{2A} receptor blockade. In order to investigate the extra-striatal D_2 receptor blockade, Pilowsky et al. [50] used ^{123}I-epidepride, a D_2/D_3 receptor tracer with higher affinity than ^{123}I-IBZM. The higher affinity was needed due to the much lower concentration of D_2 receptors outside the striatum. They found that, while typical antipsychotics produce high D_2 receptor occupancy in both striatal and extra-striatal regions (temporal cortex), Clozapine produced high occupancy only in extra-striatal regions. This could explain the clinical efficacy of atypical drugs with low Parkinsonian side-effects. However, this finding remained controversial for some time due to methodological issues, which were eventually solved [51]. The finding was also supported by the results of a

[2]No statistically significant difference.

meta-analysis, which pools data from several published PET and SPECT studies [52].

20.9 Conclusions

In this chapter, we have described the basic mathematical tools and concepts used in tracer kinetic modelling for quantification of physiological or biochemical parameters in vivo with PET or SPECT. Summaries of the basic theory discussed here can be found in [53, 54]. The next chapter will describe various methods used in practice for parameter estimation and discuss some examples of practical applications.

Appendix 1: Compartmental Models

Expressions for the impulse response functions for the 1-TC and 2-TC models are derived below. $L\{\cdot\}$ represents the Laplace transform, Laplace domain functions are identified with a tilde, and s is a complex Laplace domain variable.

1-TC Model

$$\frac{\mathrm{d}}{\mathrm{d}t}C_{\mathrm{T}}(t) = K_1 C_{\mathrm{p}}(t) - k_2'' C_{\mathrm{T}}(t)$$
$$\Leftrightarrow$$
$$L\left\{\frac{\mathrm{d}}{\mathrm{d}t}C_{\mathrm{T}}(t)\right\} = L\left\{K_1 C_{\mathrm{p}}(t) - k_2'' C_{\mathrm{T}}(t)\right\}$$
$$\Leftrightarrow$$
$$s\hat{C}_{\mathrm{T}}(s) - C_{\mathrm{T}}(0) = K_1 \hat{C}_{\mathrm{p}}(s) - k_2''\hat{C}_{\mathrm{T}}(s)$$
$$\Rightarrow$$

With initial condition, $C_T(0) = 0$:

$$\hat{C}_{\mathrm{T}}(s) = \frac{K_1}{s + k_2''}\hat{C}_{\mathrm{p}}(s)$$
$$\Leftrightarrow \qquad (20.24)$$
$$C_{\mathrm{T}}(t) = K_1 \mathrm{e}^{-k_2'' t} \otimes C_{\mathrm{p}}(t)$$
$$\Leftrightarrow$$

Impulse response function:

$$H_1(t) = K_1 \mathrm{e}^{-k_2'' t} \qquad (20.25)$$

2-TC Model

$$\frac{\mathrm{d}}{\mathrm{d}t}C_{\mathrm{ND}}(t) = K_1 C_{\mathrm{p}}(t) - \left(k_2' + k_3'\right)C_{\mathrm{ND}}(t) + k_4 C_{\mathrm{S}}(t)$$
$$\frac{\mathrm{d}}{\mathrm{d}t}C_{\mathrm{S}}(t) = k_3' C_{\mathrm{ND}}(t) - k_4 C_{\mathrm{S}}(t)$$
$$\Leftrightarrow$$
$$\begin{cases} s\hat{C}_{\mathrm{ND}}(s) - C_{\mathrm{ND}}(0) = K_1\hat{C}_{\mathrm{p}}(s) - \\ \qquad\qquad \left(k_2' + k_3'\right)\hat{C}_{\mathrm{ND}}(s) + k_4\hat{C}_{\mathrm{S}}(s) \\ s\hat{C}_{\mathrm{S}}(s) - C_{\mathrm{S}}(0) = k_3'\hat{C}_{\mathrm{ND}}(s) - k_4\hat{C}_{\mathrm{S}}(s) \end{cases}$$

With initial conditions, $C_{ND}(0) = C_S(0) = 0$:

$$\Rightarrow$$
$$\begin{cases} \left(s + k_2' + k_3'\right)\hat{C}_{\mathrm{ND}}(s) = K_1\hat{C}_{\mathrm{p}}(s) + k_4\hat{C}_{\mathrm{S}}(s) \\ \left(s + k_4\right)\hat{C}_{\mathrm{S}}(s) = k_3'\hat{C}_{\mathrm{ND}}(s) \end{cases}$$
$$\Leftrightarrow$$
$$\begin{cases} \hat{C}_{\mathrm{ND}}(s) = \left(s + k_2' + k_3' - \dfrac{k_3' k_4}{s + k_4}\right)^{-1} K_1\hat{C}_{\mathrm{p}}(s) \\ \hat{C}_{\mathrm{S}}(s) = \dfrac{k_3'}{s + k_4}\hat{C}_{\mathrm{ND}}(s) \end{cases}$$
$$\Rightarrow$$
$$\hat{C}_T(s) \equiv \hat{C}_{\mathrm{ND}}(s) + \hat{C}_{\mathrm{S}}(s) = \left(1 + \frac{k_3'}{s + k_4}\right)\hat{C}_{\mathrm{ND}}(s)$$
$$= \left(\frac{s + k_3' + k_4}{s + k_4}\right)\left(\frac{s + k_4}{\left(s + k_2' + k_3'\right)\left(s + k_4\right) - k_3' k_4}\right) K_1\hat{C}_{\mathrm{p}}(s)$$
$$= \left(\frac{s + k_3' + k_4}{s^2 + \left(k_2' + k_3' + k_4\right)s + k_2' k_4}\right) K_1\hat{C}_{\mathrm{p}}(s)$$
$$\sim\sim\sim \qquad (20.26)$$

Find poles:

$$s^2 + \left(k_2^{'} + k_3^{'} + k_4\right)s + k_2^{'}k_4 = 0$$

$$\Leftrightarrow$$

$$s = -\frac{1}{2}\left(k_2^{'} + k_3^{'} + k_4 \mp \sqrt{\left(k_2^{'} + k_3^{'} + k_4\right)^2 - 4k_2^{'}k_4}\right)$$
$$\equiv -\theta_{1,2}$$

~~~

Partial fraction expansion:

$$\frac{\phi_1}{s+\theta_1} + \frac{\phi_2}{s+\theta_2} = K_1 \frac{s + k_3^{'} + k_4}{s^2 + \left(k_2^{'} + k_3^{'} + k_4\right)s + k_2^{'}k_4} \tag{20.27}$$

$$\Leftrightarrow$$

$$\begin{cases} \phi_1 = K_1 \dfrac{k_3^{'} + k_4 - \theta_1}{\theta_2 - \theta_1} \\ \phi_2 = -K_1 \dfrac{k_3^{'} + k_4 - \theta_2}{\theta_2 - \theta_1} \end{cases}$$

~~~

$$(20.26) + (20.27)$$

$$\Rightarrow$$

$$\hat{C}_{\mathrm{T}}(s) = \left(\frac{\phi_1}{s+\theta_1} + \frac{\phi_2}{s+\theta_2}\right)\hat{C}_{\mathrm{p}}(s) \tag{20.28}$$

$$\Leftrightarrow$$

$$C_{\mathrm{T}}(t) = \left(\phi_1 \mathrm{e}^{-\theta_1 t} + \phi_2 \mathrm{e}^{-\theta_2 t}\right) \otimes C_{\mathrm{p}}(t)$$

$$\Leftrightarrow$$

Impulse response function:

$$H_2(t) = \phi_1 \mathrm{e}^{-\theta_1 t} + \phi_2 \mathrm{e}^{-\theta_2 t} \tag{20.29}$$

Appendix 2: Reference Tissue Models

1-TC Model

$$\begin{cases} \dfrac{\mathrm{d}}{\mathrm{d}t} C_{\mathrm{T}}(t) = K_1 C_{\mathrm{p}}(t) - k_2^{''} C_{\mathrm{T}}(t) \\ \dfrac{\mathrm{d}}{\mathrm{d}t} C_{\mathrm{R}}(t) = {}^{R}K_1 C_{\mathrm{p}}(t) - {}^{R}k_2^{'} C_{\mathrm{R}}(t) \end{cases}$$

$$\Leftrightarrow$$

From Eq. (20.24):

$$\begin{cases} \hat{C}_{\mathrm{T}}(s) = \dfrac{K_1}{s + k_2^{''}} \hat{C}_{\mathrm{p}}(s) \\ \hat{C}_{\mathrm{R}}(s) = \dfrac{{}^{R}K_1}{s + {}^{R}k_2^{'}} \hat{C}_{\mathrm{p}}(s) \end{cases}$$

$$\Rightarrow$$

$$\left(\text{with } R_1 = \frac{K_1}{{}^{R}K_1}\right):$$

$$\hat{C}_{\mathrm{T}}(s) = R_1 \frac{s + {}^{R}k_2^{'}}{s + k_2^{''}} \hat{C}_{\mathrm{R}}(s)$$

$$= R_1 \hat{C}_{\mathrm{R}}(s) + R_1 \frac{{}^{R}k_2^{'} - k_2^{''}}{s + k_2^{''}} \hat{C}_{\mathrm{R}}(s)$$

$$\Rightarrow$$

$$C_{\mathrm{T}}(t) = R_1 C_{\mathrm{R}}(t) + R_1 \left({}^{R}k_2^{'} - k_2^{''}\right)\mathrm{e}^{-k_2^{''}t} \otimes C_{\mathrm{R}}(t)$$

$$\Leftrightarrow$$

Impulse response function:

$$H_{1\mathrm{R}}(t) = R_1 \delta(t) + R_1 \left({}^{R}k_2^{'} - k_2^{''}\right)\mathrm{e}^{-k_2^{''}t} \tag{20.30}$$

where $\delta(t)$ is the Dirac delta-function.

2-TC model

$$\begin{cases} \frac{\mathrm{d}}{\mathrm{d}t}C_{\mathrm{ND}}(t) = K_1 C_{\mathrm{p}}(t) - \left(k_2^{'} + k_3^{'}\right) C_{\mathrm{ND}}(t) \\ \qquad\qquad + k_4 C_{\mathrm{S}}(t) \\ \frac{\mathrm{d}}{\mathrm{d}t}C_{\mathrm{S}}(t) = k_3^{'} C_{\mathrm{ND}}(t) - k_4 C_{\mathrm{S}}(t) \\ \frac{\mathrm{d}}{\mathrm{d}t}C_{\mathrm{R}}(t) = {}^{R}K_1 C_{\mathrm{p}}(t) - {}^{R}k_2^{'} C_{\mathrm{R}}(t) \end{cases}$$

From Eqs. (20.24) and (20.28):

$$\begin{cases} \hat{C}_{\mathrm{T}}(s) = \left(\frac{\phi_1}{s+\theta_1} + \frac{\phi_2}{s+\theta_2}\right)\hat{C}_{\mathrm{p}}(s) \\ \hat{C}_{\mathrm{R}}(s) = \frac{{}^{R}K_1}{s+{}^{R}k_2^{'}}\hat{C}_{\mathrm{p}}(s) \end{cases}$$

$$\Rightarrow$$

$$\hat{C}_{\mathrm{T}}(s) = \left(\frac{\phi_1}{s+\theta_1} + \frac{\phi_2}{s+\theta_2}\right)\frac{s+{}^{R}k_2^{'}}{{}^{R}K_1}\hat{C}_{\mathrm{R}}(s)$$

$$\Leftrightarrow$$

$$\left(\text{with } R_1 = \frac{K_1}{{}^{R}K_1}\right):$$

$$\begin{aligned} \hat{C}_{\mathrm{T}}(s) &= \frac{R_1}{\theta_2-\theta_1}\left(\frac{k_3^{'}+k_4-\theta_1}{s+\theta_1} - \frac{k_3^{'}+k_4-\theta_2}{s+\theta_2}\right)\left(s+{}^{R}k_2^{'}\right)\hat{C}_{\mathrm{R}}(s) \\ &= \frac{R_1}{\theta_2-\theta_1} \\ &\quad \left(\left(k_3^{'}+k_4-\theta_1\right)\left(1+\frac{{}^{R}k_2^{'}-\theta_1}{s+\theta_1}\right) - \left(k_3^{'}+k_4-\theta_2\right)\left(1+\frac{{}^{R}k_2^{'}-\theta_2}{s+\theta_2}\right)\right)\hat{C}_{\mathrm{R}}(s) \\ &= R_1\hat{C}_{\mathrm{R}}(s) + \frac{R_1}{\theta_2-\theta_1} \\ &\quad \left(\frac{\left(k_3^{'}+k_4-\theta_1\right)\left({}^{R}k_2^{'}-\theta_1\right)}{s+\theta_1} - \frac{\left(k_3^{'}+k_4-\theta_2\right)\left({}^{R}k_2^{'}-\theta_2\right)}{s+\theta_2}\right)\hat{C}_{\mathrm{R}}(s) \end{aligned}$$

$$\Leftrightarrow$$

$$\hat{C}_{\mathrm{T}}(s) = R_1\hat{C}_{\mathrm{R}}(s) + \left(\frac{\rho_1}{s+\theta_1} + \frac{\rho_2}{s+\theta_2}\right)\hat{C}_{\mathrm{R}}(s) \tag{20.31}$$

where

$$\begin{cases} \rho_1 = R_1\frac{\left(k_3^{'}+k_4-\theta_1\right)\left({}^{R}k_2^{'}-\theta_1\right)}{\theta_2-\theta_1} \\ \rho_2 = -R_1\frac{\left(k_3^{'}+k_4-\theta_2\right)\left({}^{R}k_2^{'}-\theta_2\right)}{\theta_2-\theta_1} \end{cases}$$

$$\sim\sim\sim$$

$$(20.31)$$

$$\Rightarrow$$

$$C_{\mathrm{T}}(t) = R_1 C_{\mathrm{R}}(t) + \left(\rho_1 \mathrm{e}^{-\theta_1 t} + \rho_2 \mathrm{e}^{-\theta_2 t}\right) \otimes C_{\mathrm{R}}(t)$$

$$\Leftrightarrow$$

Impulse response function:

$$H_{2\mathrm{R}}(t) = R_1\delta(t) + \rho_1 \mathrm{e}^{-\theta_1 t} + \rho_2 \mathrm{e}^{-\theta_2 t} \tag{20.32}$$

Appendix 3: Logan Graphical Analysis

1-TC Model

$$\frac{\mathrm{d}}{\mathrm{d}t}C_{\mathrm{T}}(t) = K_1 C_{\mathrm{p}}(t) - k_2^{''} C_{\mathrm{T}}(t)$$

$$\Leftrightarrow$$

$$C_{\mathrm{T}}(t) - C_{\mathrm{T}}(0) = K_1\int_0^t C_{\mathrm{p}}(\tau)\,\mathrm{d}\tau - k_2^{''}\int_0^t C_{\mathrm{T}}(\tau)\,\mathrm{d}\tau$$

with $C_{\mathrm{T}}(0) = 0$:

$$\Leftrightarrow$$

$$\frac{\int_0^t C_{\mathrm{T}}(\tau)\,\mathrm{d}\tau}{C_{\mathrm{T}}(t)} = \frac{K_1}{k_2^{''}}\frac{\int_0^t C_{\mathrm{p}}(\tau)\,\mathrm{d}\tau}{C_{\mathrm{T}}(t)} - \frac{1}{k_2^{''}}$$

$$\Rightarrow$$

$$\frac{\int_0^t C_T(\tau)\,d\tau}{C_T(t)} = V_T \frac{\int_0^t C_p(\tau)\,d\tau}{C_T(t)} + \text{const.} \tag{20.33}$$

2-TC Model

$$\begin{cases} \frac{d}{dt} C_{ND}(t) = K_1 C_p(t) - \left(k_2' + k_3'\right) C_{ND}(t) + k_4 C_S(t) \\ \frac{d}{dt} C_S(t) = k_3' C_{ND}(t) - k_4 C_S(t) \end{cases}$$

$$\Leftrightarrow$$

$$\begin{cases} C_{ND}(t) - C_{ND}(0) = \\ K_1 \int_0^t C_p(\tau)\,d\tau - \left(k_2' + k_3'\right) \int_0^t C_{ND}(\tau)\,d\tau \\ + k_4 \int_0^t C_S(\tau)\,d\tau \\ C_S(t) - C_S(0) = k_3' \int_0^t C_{ND}(t)\,d\tau - k_4 \int_0^t C_S(\tau)\,d\tau \end{cases}$$

with $C_{ND}(0) = C_S(0) = 0$:

$$\Leftrightarrow$$

$$\begin{cases} C_T(t) = K_1 \int_0^t C_p(\tau)\,d\tau - k_2' \int_0^t C_{ND}(\tau)\,d\tau \\ C_S(t) = k_3' \int_0^t C_{ND}(\tau)\,d\tau - k_4 \int_0^t C_S(\tau)\,d\tau \end{cases}$$

$$\Leftrightarrow$$

$$\begin{cases} \frac{\int_0^t C_{ND}(\tau)\,d\tau}{C_T(t)} = \frac{K_1}{k_2'} \frac{\int_0^t C_P(\tau)\,d\tau}{C_T(t)} - \frac{1}{k_2'} \\ \frac{\int_0^t C_S(\tau)\,d\tau}{C_T(t)} = \frac{k_3'}{k_4} \frac{\int_0^t C_{ND}(\tau)\,d\tau}{C_T(t)} - \frac{1}{k_4} \frac{C_S(t)}{C_T(t)} \end{cases}$$

$$\Rightarrow$$

$$\begin{aligned} \frac{\int_0^t C_T(\tau)\,d\tau}{C_T(t)} &\equiv \frac{\int_0^t C_{ND}(\tau) + C_S(\tau)\,d\tau}{C_T(t)} \\ &= \frac{K_1}{k_2'} \frac{\int_0^t C_P(\tau)\,d\tau}{C_T(t)} - \frac{1}{k_2'} \\ &\quad + \frac{k_3'}{k_4} \left(\frac{K_1}{k_2'} \frac{\int_0^t C_P(\tau)\,d\tau}{C_T(t)} - \frac{1}{k_2'} \right) - \frac{1}{k_4} \frac{C_S(t)}{C_T(t)} \\ &= \frac{K_1}{k_2'} \left(1 + \frac{k_3'}{k_4} \right) \frac{\int_0^t C_P(\tau)\,d\tau}{C_T(t)} \\ &\quad - \frac{1}{k_2'} \left(1 + \frac{k_3'}{k_4} \right) - \frac{1}{k_4} \frac{C_S(t)}{C_T(t)} \end{aligned}$$

$$\Leftrightarrow$$

$$\frac{\int_0^t C_T(\tau)\,d\tau}{C_T(t)} = V_T \frac{\int_0^t C_P(\tau)\,d\tau}{C_T(t)} - \frac{1}{k_2''} - \frac{1}{k_4} \frac{C_S(t)}{C_T(t)}$$

$$\Rightarrow$$

with $C_S(t)/C_T(t) = \text{constant}$ (pseudo-equilibrium):

$$\frac{\int_0^t C_T(\tau)\,d\tau}{C_T(t)} = V_T \frac{\int_0^t C_P(\tau)\,d\tau}{C_T(t)} + \text{const.} \tag{20.34}$$

References

1. Cunningham VJ, Gunn RN, Matthews JC. Quantification in positron emission tomography for research in pharmacology and drug development. Nucl Med Commun. 2004;25:643–6.
2. Laruelle M. The role of model-based methods in the development of single scan techniques. Nucl Med Biol. 2000;27:637–42.
3. Erlandsson K, Buvat I, Pretorius PH, Thomas BA, Hutton BF. A review of partial volume correction techniques for emission tomography and their applications in neurology, cardiology and oncology. Phys Med Biol. 2012;57:R119–59.

4. Carson RE. The development and application of mathematical models in nuclear medicine. J Nucl Med. 1991;32:2206–8.
5. Carson RE. Tracer kinetic modelling in PET. In: Valk PE, Bailey DL, Townsend DW, Maisey MN, editors. Positron emission tomography: basic science and clinical practice. London: Springer-Verlag; 2003. p. 147–79.
6. Gunn RN, Gunn SR, Cunningham VJ. Positron emission tomography compartmental models. J Cereb Blood Flow Metab. 2001;21:635–52.
7. Arfken G. Mathematical methods for physicists. San Diego: Academic; 1985.
8. Kety SS, Schmidt CF. The nitrous oxide method for the quantitative determination of cerebral blood flow in man: theory, procedure and normal values. J Clin Invest. 1948;27:476–83.
9. Kety SS. The theory and applications of the exchange of inert gas at the lungs and tissues. Pharmacol Rev. 1951;3:1–41.
10. Renkin EM. Transport of potassium-42 from blood to tissue in isolated mammalian skeletal muscles. Am J Phys. 1959;197:1205–10.
11. Crone C. The permeability of capillaries in various organs as determined by use of the 'indicator diffusion' method. Acta Physiol Scand. 1963;58:292–305.
12. Kerwin RW, Pilowsky LS. Traditional receptor theory and its application to neuroreceptor measurements in functional imaging. Eur J Nucl Med. 1995;22:699–710.
13. Michaelis L, Menten ML. Die kinetik der invertinwirkung. Biochem Z. 1913;49:1333.
14. Scatchard G. The attractions of proteins for small molecules and ions. Ann N Y Acad Sci. 1949;51:660–5.
15. Mintun MA, Raichle ME, Kilbourn MR, Wooten GF, Welch MJ. A quantitative model for the in vivo assessment of drug binding sites with positron emission tomography. Ann Neurol. 1984;15:217–27.
16. Scheibe PO. Identifiability analysis of second-order systems. Nucl Med Biol. 2003;30:827–32.
17. Koeppe RA, Holthoff VA, Frey KA, Kilbourn MR, Kuhl DE. Compartmental analysis of [^{11}C]flumazenil kinetics for the estimation of ligand transport rate and receptor distribution using positron emission tomography. J Cereb Blood Flow Metab. 1991;11:735–44.
18. Erlandsson K, Bressan RA, Mulligan RS, Gunn RN, Cunningham VJ, Owens J, Wyper D, Ell PJ, Pilowsky LS. Kinetic modelling of [^{123}I]-CNS 1261—a novel SPET tracer for the NMDA receptor. Nucl Med Biol. 2003;30:441–54.
19. Tonietto M, Rizzo G, Veronese M, Fujita M, Zoghbi SS, Zanotti-Fregonara P, Bertoldo A. Plasma radiometabolite correction in dynamic PET studies: insights on the available modeling approaches. J Cereb Blood Flow Metab. 2016;36:326–39.
20. Zanotti-Fregonara P, Fadaili EM, Maroy R, Comtat C, Souloumiac A, Jan S, Ribeiro M-J, Gaura V, Bar-Hen A, Trebossen R. Comparison of eight methods for the estimation of the image-derived input function in dynamic [^{18}F]-FDG PET human brain studies. J Cereb Blood Flow Metab. 2009;29:1825–35.
21. Sari H, Erlandsson K, Law I, Larsson HB, Ourselin S, Arridge S, Atkinson D, Hutton BF. Estimation of an image derived input function with MR-defined carotid arteries in FDG-PET human studies using a novel partial volume correction method. J Cereb Blood Flow Metab. 2017;37:1398–409.
22. Innis RB, Cunningham VJ, Delforge J, Fujita M, Gjedde A, Gunn RN, Holden J, Houle S, Huang SC, Ichise M, Iida H, Ito H, Kimura Y, Koeppe RA, Knudsen GM, Knuuti J, Lammertsma AA, Laruelle M, Logan J, Maguire RP, Mintun MA, Morris ED, Parsey R, Price JC, Slifstein M, Sossi V, Suhara T, Votaw JR, Wong DF, Carson RE. Consensus nomenclature for in vivo imaging of reversibly binding radioligands. J Cereb Blood Flow Metab. 2007;27:1533–9.
23. Marquardt DW. An algorithm for least-squares estimation of nonlinear parameters. J Soc Ind Appl Math. 1963;11:431–41.
24. Press WH, Teukolsky SA, Vetterling WT, Flannery BP. Numerical recipies in C: the art of scientific computing. Cambridge: Cambridge University Press; 1992.
25. Feng D, Wong K-P, Wu C-M, Siu W-C. A technique for extracting physiological parameters and the required input function simultaneously from PET image measurements: theory and simulation study. IEEE Trans Inform Technol Biomed. 1997;1:243–54.
26. Cunningham VJ, Hume SP, Price GR, Ahier RG, Cremer JE, Jones AK. Compartmental analysis of diprenorphine binding to opiate receptors in the rat in vivo and its comparison with equilibrium data in vitro. J Cereb Blood Flow Metab. 1991;11:1–9.
27. Lammertsma AA, Bench CJ, Hume SP, Osman S, Gunn K, Brooks DJ, Frackowiak RS. Comparison of methods for analysis of clinical [^{11}C]raclopride studies. J Cereb Blood Flow Metab. 1996;16:42–52.
28. Lammertsma AA, Hume SP. Simplified reference tissue model for PET receptor studies. NeuroImage. 1996;4:153–8.
29. Wu Y, Carson RE. Noise reduction in the simplified reference tissue model for neuroreceptor functional imaging. J Cereb Blood Flow Metab. 2002;22:1440–52.
30. Erlandsson K, Sivananthan T, Lui D, Spezzi A, Townsend CE, Mu S, Lucas R, Warrington S, Ell PJ. Measuring SSRI occupancy of SERT using the novel tracer [^{123}I]ADAM: a SPECT validation study. Eur J Nucl Med Mol Imaging. 2005;32:1329–36.
31. Cunningham VJ, Jones T. Spectral analysis of dynamic PET studies. J Cereb Blood Flow Metab. 1993;13:15–23.
32. Gunn RN, Gunn SR, Turkheimer FE, Aston JAD, Cunningham VJ. Positron emission tomography compartmental models: a basis pursuit strategy for kinetic modelling. J Cereb Blood Flow Metab. 2002;22:1425–39.
33. Logan J, Fowler JS, Volkow ND, Wolf AP, Dewey SL, Schlyer DJ, MacGregor RR, Hitzemann R, Bendriem

B, Gatley SJ, et al. Graphical analysis of reversible radioligand binding from time-activity measurements applied to [N-^{11}C-methyl]-(−)-cocaine PET studies in human subjects. J Cereb Blood Flow Metab. 1990;10:740–7.
34. Slifstein M, Laruelle M. Effects of statistical noise on graphic analysis of PET neuroreceptor studies. J Nucl Med. 2000;41:2083–8.
35. Ogden RT. Estimation of kinetic parameters in graphical analysis of PET imaging data. Stat Med. 2003;22:3557–68.
36. Logan J, Fowler JS, Volkow ND, Wang GJ, Ding YS, Alexoff DL. Distribution volume ratios without blood sampling from graphical analysis of PET data. J Cereb Blood Flow Metab. 1996;16:834–40.
37. Patlak CS, Blasberg RG, Fenstermacher JD. Graphical evaluation of blood-to-brain transfer constants from multiple-time uptake data. J Cereb Blood Flow Metab. 1983;3:1–7.
38. Rahmim A, Lodge MA, Karakatsanis NA, Panin VY, Zhou Y, McMillan A, Cho S, Zaidi H, Casey ME, Wahl RL. Dynamic whole-body PET imaging: principles, potentials and applications. Eur J Nucl Med Mol Imaging. 2019;46:501–18.
39. Carson RE. PET physiological measurements using constant infusion. Nucl Med Biol. 2000;27:657–60.
40. Carson RE, Channing MA, Blasberg RG, Dunn BB, Cohen RM, Rice KC, Herscovitch P. Comparison of bolus and infusion methods for receptor quantitation: application to [^{18}F]cyclofoxy and positron emission tomography. J Cereb Blood Flow Metab. 1993;13:24–42.
41. Kawai R, Carson RE, Dunn B, Newman AH, Rice KC, Blasberg RG. Regional brain measurement of Bmax and KD with the opiate antagonist cyclofoxy: equilibrium studies in the conscious rat. J Cereb Blood Flow Metab. 1991;11:529–44.
42. Holden JE, Jivan S, Ruth TJ, Doudet DJ. In vivo receptor assay with multiple ligand concentrations: an equilibrium approach. J Cereb Blood Flow Metab. 2002;22:1132–41.
43. Bressan RA, Erlandsson K, Mulligan RS, Gunn RN, Cunningham VJ, Owens J, Cullum ID, Ell PJ, Pilowsky LS. A bolus/infusion paradigm for the novel NMDA receptor SPET tracer [^{123}I]CNS 1261. Nucl Med Biol. 2004;31:155–64.
44. Akaike H. A new look at the statistical model identification. IEEE Trans Automat Contr. 1974;19:716–23.
45. Cunningham VJ. Non-linear regression techniques in data analysis. Med Inf (Lond). 1985;10:137–42.
46. Schwarz G. Estimating the dimension of a model. Ann Stat. 1978;6:461–4.
47. Ogden RT, Ojha A, Erlandsson K, Oquendo MA, Mann JJ, Parsey RV. In vivo quantification of serotonin transporters using [^{11}C]DASB and positron emission tomography in humans: modeling considerations. J Cereb Blood Flow Metab. 2007;27:205–17.
48. Pilowsky LS, Costa DC, Ell PJ, Murray RM, Verhoeff NP, Kerwin RW. Clozapine, single photon emission tomography, and the D2 dopamine receptor blockade hypothesis of schizophrenia. Lancet. 1992;340:199–202.
49. Travis MJ, Busatto GF, Pilowsky LS, Mulligan R, Acton PD, Gacinovic S, Mertens J, Terriere D, Costa DC, Ell PJ, Kerwin RW. 5-HT2A receptor blockade in patients with schizophrenia treated with risperidone or clozapine. A SPET study using the novel 5-HT2A ligand ^{123}I-5-I-R-91150. Br J Psychiatry. 1998;173:236–41.
50. Pilowsky LS, Mulligan RS, Acton PD, Ell PJ, Costa DC, Kerwin RW. Limbic selectivity of clozapine. Lancet. 1997;350:490–1.
51. Erlandsson K, Bressan RA, Mulligan RS, Ell PJ, Cunningham VJ, Pilowsky LS. Analysis of D2 dopamine receptor occupancy with quantitative SPET using the high-affinity ligand [^{123}I]epidepride: resolving conflicting findings. NeuroImage. 2003;19:1205–14.
52. Stone JM, Davis JM, Leucht S, Pilowsky LS. Cortical dopamine D2/D3 receptors are a common site of action for antipsychotic drugs--an original patient data meta-analysis of the SPECT and PET in vivo receptor imaging literature. Schizophr Bull. 2009;35(4):789–97.
53. Ichise M, Meyer JH, Yonekura Y. An introduction to PET and SPECT neuroreceptor quantification models. J Nucl Med. 2001;42:755–63.
54. Slifstein M, Laruelle M. Models and methods for derivation of in vivo neuroreceptor parameters with PET and SPECT reversible radiotracers. Nucl Med Biol. 2001;28:595–608.